*Science Journal of Chemistry*
2025, Vol. 13, No. 3, pp. 65-75
https://doi.org/10.11648/j.sjc.20251303.13

Editorial

# Azo-Imino Tautomerism in Sudan Red 7B/Cyclodextrin Coated ZnO Nanocomposites: Evidence by Spectral and Microscopic Perspectives

**Palanichamy Ramasamy[1], Narayanasamy Rajendiran[1, *], Ayyadurai Mani[2], Govindaraj Venkatesh[3], Albert Antony Muthu Prabhu[4]**

[1]Department of Chemistry, Annamalai University, Annamalai Nagar, Tamilnadu, India
[2]Center for Advanced Energy Materials, SRM TRP Engineering College, Tiruchy, India
[3]Department of Chemistry, Knowledge Institute of Technology (Autonomous), Salem, India
[4]Department of Chemistry, Aditanar College of Arts and Science, Tiruchendur, India

## Abstract

Sudan Red-7B/Cyclodextrin doped ZnO nanocomposites are synthesized and analyzed by various spectral and microscopic methods. The doping effect of SR7B/CD on ZnO nano investigated by UV-visible, fluorescence, FTIR, DTA, XRD, FE-SEM and TEM methods. The effect of different polarities of the solvents, α-cyclodextrin (α-CD) and β-cyclodextrin (β-CD), on MV was studied by various spectral methods. The inclusion behaviour of SR7B on both CDs was determined by PM3 method. The solvent and CD studies show that the azo-imino tautomer is present in the SR7B molecule and that, depending upon the polarity of the solvents, absorbance and emission intensities of the azo-imino tautomer is varied. With increasing CD concentrations, the shorter wavelength emission intensity of the SR7B regularly increased while the longer wavelength emission intensity decreased. The horizontal bond length of SR7B is longer than the CD cavities; hence, this molecule is partially encapsulated in the CD cavity. HOMO-LUMO gap for MV/β-CD inclusion complex was more negative, which supports that this complex is more stable than MV/α-CD inclusion complex. Red or blue shifted absorption and fluorescence maxima were seen in SR7B/CD/ZnO nanocomposites than SR7B/CD inclusion complex. Nanoparticle size was measured by TEM-EDS and X-RD methods. TEM image showed that nanosheets are formed in SR7B/CD/ZnO.

## Keywords

Sudan Red-7B, Tautomer, Zinc Oxide Nano, Cyclodextrin, Inclusion Complex

## 1. Introduction

The azo (A)-hydrazone (H) tautomerism of the phenyl azo naphthols was observed in the case of 1-phenylazo-4-naphthol by Zince and Bindenwald [1] over one century ago and has been explained by the existence of a `movable' proton in the molecule [2]. Unfortunately, due to the high proton exchange rate, both tautomeric forms cannot

*Corresponding author: drrajendiran1967@gmail.com (Narayanasamy Rajendiran)

**Received:** 9 May 2025; **Accepted:** 23 May 2025; **Published:** 23 June 2025

be separated experimentally, and therefore it was, for some time, impossible to investigate exactly tautomer-solvent interactions [3, 22]. The spectrophotometric analysis of tautomeric equilibria [5-22] and the solvent influence on the A-H tautomerism of some derivatives of 1 were investigated quantitatively, and it was found that the tautomeric ratio increases from non-polar to polar solvents. This general trend is also valid in the case of the isomeric 1-phenylazo-2-naphthol and 2-phenylazo-1-naphthol, but the solvent effect is not so pronounced because of the stabilizing intramolecular hydrogen bonding [6, 19-21]. From the above cited results, it is clear that there is no relation between KT and the dielectric constants of the solvents, suggesting specific interactions.

Proton tautomerism plays an important role in many fields of chemistry and especially biochemistry [1-22]. It is well known that the proton transfer can occur in the ground and/or excited state, but only during the last decade has the excited state proton transfer been the subject of substantial interest [3-9]. Molecules giving rise to excited state tautomer's by intramolecular proton transfer (IPT) are often used as laser dyes, in higher energy radiation detectors and molecular memory storage devices, as fluorescent probes, and polymer protectors [10, 11].

Zinc oxide nanoparticles are low in toxicity and have high UV absorption are used in various fields like the ceramic industry, biomedical, etc, because they act as a good surface material. [23-37]. It has a hard, rigid structure and is naturally known to have a strong resistance to microbes [23]. Due to these reasons, zinc oxide nanoparticles are extensively used for biological labeling, biological sensing, drug delivery, gene delivery, and nanomedicine [24]. The Food and drug administration has approved zinc oxide as a safe material. Zinc oxide can also be solubilized in an acidic environment; therefore, this allows the material to be discovered as multifunctional nanocarriers to ease the drug delivery and release processes. Because of the above reasons, this manuscript focuses on: a) analyzing the type of tautomer present in the Sudan Red-7B, b) synthesizing and characterizing ZnO, CD/ZnO, SR7B/ZnO, and SR7B/CD/ZnO nanomaterials using various spectral and microscopic techniques, and c) studying the doping effect of the SR7B/CD on ZnO nanoparticles.

## 2. Experimental

### 2.1. Preparation of Drug/CD Inclusion Complex in Solution

Different concentrations of α-CD or β-CD solution (0.1 to $1.0\times10^{-2}$ M) were taken in 10 ml standard measuring flask. SR7B stock solution has a concentration of $2\times10^{-2}$ M. 0.2 ml of the SR7B stock solution was added to the above flasks. The mixed solution was made up to 10 ml with triple-distilled water and shaken very well. The final SR7B concentration in each flask was $4\times10^{-4}$ M and 298 K temperature was used for the experiments.

### 2.2. Preparation of ZnO and ZnO /SR7B/CD Nanomaterials

0.01 M of zinc sulphate dissolved in 100 ml of deionized water was to heated 50 - 60 ℃ for 20 to 30 minutes. $ZnSO_4$ and NaOH (1%) solution with a molar ratio of 1: 2, which was carried out under vigorous stirring for 12 h at room temperature. The obtained white ZnO precipitate was washed several times and separated by centrifugation [36-42] and dried in an oven at 100 ℃ for 6h. The prepared ZnO nanoparticles showed a size distribution of about 25-50 nm.

SR7B ($2\times10^{-3}$ M) was dissolved in 20 ml of ethanol and gradually added to the CD ($1\times10^{-2}$ M in 80 ml) in deionized water. Then this SR7B/CD solution was added to the 0.01 M zinc sulphate (100 ml) Using a hot plate with a magnetic stirrer, this mixture was heated to 50 ℃ for one hour. With vigorous stirring, one to two ml of 1% sodium hydroxide was added and stirred for one to two hours. After that, the above solution was frozen and dried (mini-lyophilized) at -80 ℃. The powder SR7B/CD/ZnO sample was collected and used for further analysis.

$$\underset{(0.01\ M\ in\ 100\ ml\ H_2O)}{ZnSO_4} + \underset{(5\ ml)}{1\%\ NaOH} \rightarrow \underset{(White\ precipitate)}{ZnO\ nano}$$

$$\underset{(0.1\ M)}{CD} + \underset{(0.002\ M)}{SR7B} \rightarrow SR7B/CD\ inclusion\ complex$$

$$\underset{(0.01\ M\ 100\ ml)}{ZnSO_4} + \underset{(100\ ml)}{SR7B/CD} + \underset{(5\ ml)}{1\%\ NaOH} \rightarrow \underset{(White\ precipitate)}{SR7B/CD/ZnO\ nano}$$

## 2.3. Molecular Modeling Studies

Using the molecular modeling software Spartan 08, the molecular geometry of SR7B, CD and its inclusion complexes were analyzed. The most stable complexation energy was determined theoretically after the structural assembly of two orientation inclusion complexes using the semi-empirical PM3 method in the gas phase and Gaussian 09W software.

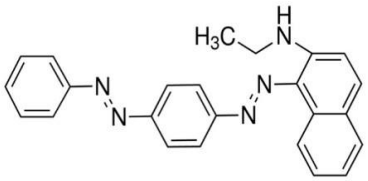


***Figure 1.*** *Chemical structure of sudan red-7B [SR7B].*

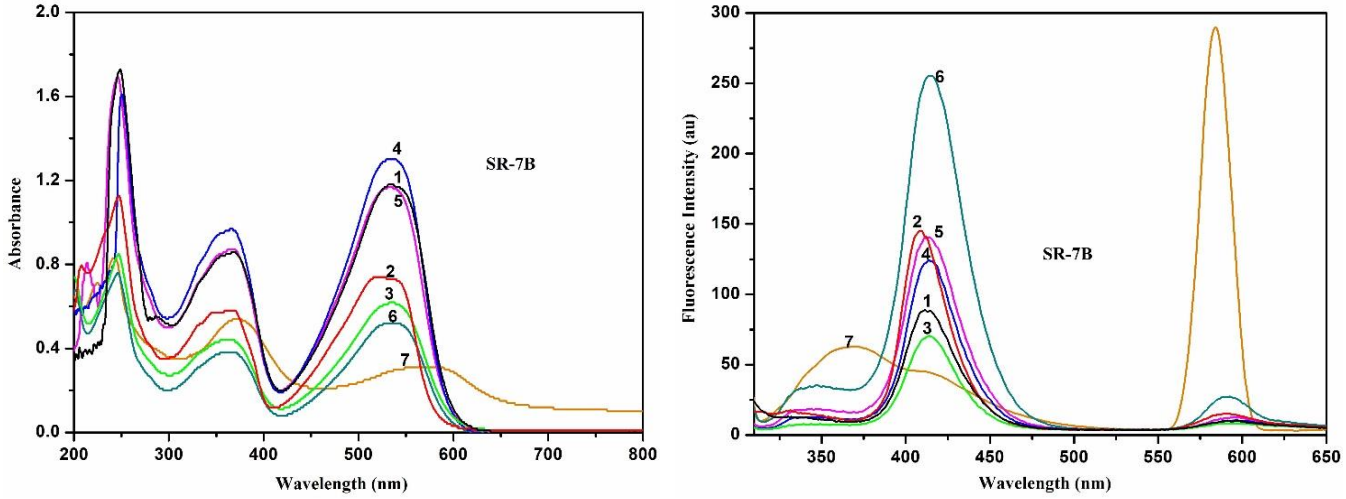


***Figure 2.*** *Absorption and fluorescence spectra of SR7B in different solvents at 303 K: 1) cyclohexane 2) 1, 4-dioxane 3) ethyl acetate 4) acetonitrile 5) 2-propanol 6) ethanol 7) water.*

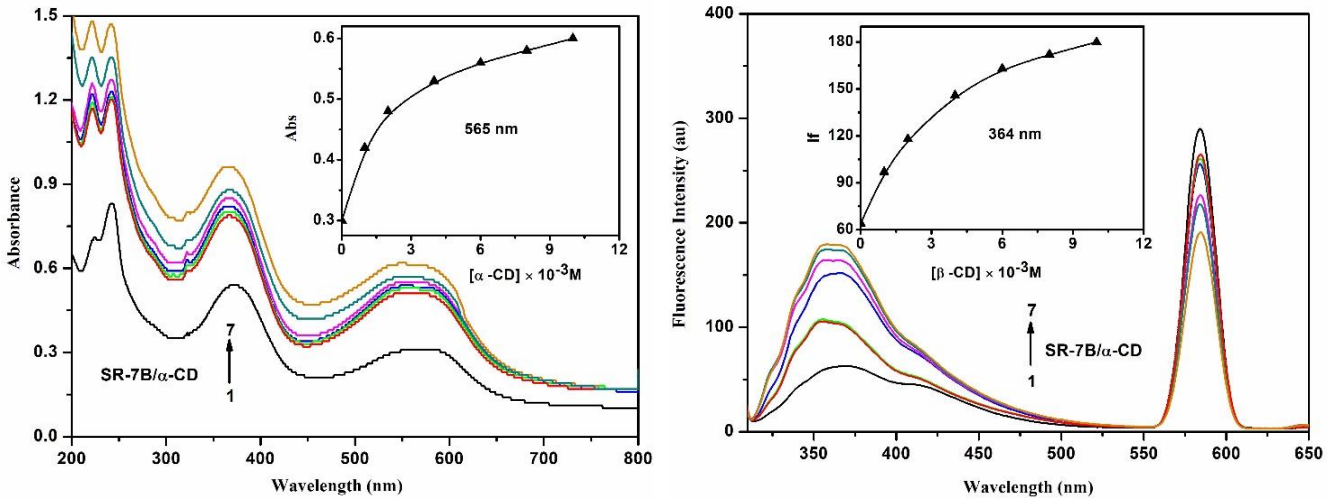


***Figure 3.*** *Absorption and fluorescence spectra of SR7B in different α-CD concentrations (M): (1) 0, (2) 0.001, (3) 0.002, (4) 0.004, (5) 0.006, (6) 0.008, (7) 0.01. Insert figure: absorbance/IF vs [α-CD].*

# 3. Result and Discussion

## 3.1. Effect of Solvents and Cyclodextrins

The absorption and emission spectra of sudan red-7B (*N*-Ethyl-1-{[4-(phenyl diazenyl) phenyl] diazenyl}naphthalen-2-amine, SR7B, Figure 1) were examined in different solvents and α-CD and β-CD solutions (Table 1, Figures 2 and 3). In all the solvents, α-CD and β-CD solutions, three absorption and two emission spectral maxima are observed in SR7B (Table 1) which is similar to that observed in

other azo compounds [16-22]. The absorption and emission maxima of SR7B are red shifted from nonpolar (cyclohexane: $\lambda_{abs}$~ 521, 367, 247 nm, $\lambda_{emi}$~591, 410 nm) to polar solvents, however, large red shift is observed in water ($\lambda_{abs}$~ 565, 368, 244, 224 nm, $\lambda_{emi}$~584, 364 nm). The data reveal that the location of both bands is relatively influenced by the nature of the substituent and the polarity of the solvents. The absorption and emission spectral shifts of SR7B in all the solvents are different from the CD solution, suggesting that SR7B molecule is encapsulated in the CD cavity. The bathochromic or hypsochromic shifts in the ground and excited state reflect increased delocalization of the N=N group and π-cloud of the aromatic ring [16-22].

***Table 1.*** *Absorption and fluorescence spectral maxima of SR7B with different Solvents and cyclodextrins.*

| Solvents | $\lambda_{abs}$ | log ε | $\lambda_{flu}$ |
|---|---|---|---|
| Cyclohexane | 521 | 3.27 | 591 |
| | 367 | 3.17 | 410 |
| | 247 | 3.46 | |
| 1, 4-Dioxane | 534 | 3.48 | 591 |
| | 369 | 3.34 | 412 |
| | 248 | 3.64 | |
| Ethyl acetate | 534 | 3.52 | 597 |
| | 365 | 3.39 | 414 |
| | 250 | 3.61 | |
| Acetonitrile | 534 | 3.20 | 595 |
| | 364 | 3.05 | 414 |
| | 247 | 3.33 | |
| 2-Propanol | 533 | 3.47 | 414 |
| | 366 | 3.34 | 598 |
| | 246 | 3.63 | |
| Ethanol | 536 | 3.12 | 593 |
| | 366 | 2.98 | 414 |
| | 246 | 3.28 | |
| Water | 565 | 2.88 | 584 |
| | 368 | 3.13 | 364 |
| | 244 | 3.32 | |
| | 224 | 3.25 | |
| α-CD -0.01 M | 562 | 3.18 | 584 |
| | 365 | 3.39 | 362 |
| | 242 | 3.57 | |
| | 222 | 3.57 | |
| β-CD 0.01 M | 563 | 3.17 | 584 |
| | 366 | 3.35 | 363 |
| | 243 | 3.53 | |
| | 223 | 3.53 | |
| α-CD K (1: 1) x$10^5$ $M^{-1}$ | 54 | - | 139 |
| β-CD K (1: 1) x$10^5$ $M^{-1}$ | 144 | - | 176 |
| α-CD ΔG (kcal$mol^{-1}$) | -11.0 | - | -13.4 |
| β-CD ΔG (kcal$mol^{-1}$) | -13.5 | - | -14.0 |
| Excitation wavelength (nm) | - | - | 320 |

Upon increasing the CD concentrations, i) the absorption appear in water (565, 368, 244, 222 nm) slightly blue shifted and the absorbance regularly increased, ii) in the excited state dual emission noted at 584, 366 nm, iii) the shorter wavelength emission maxima regularly increased with slight blue shift, whereas the longer wavelength emission intensity decreased at the same wavelength, and iv) the CD cavity provide a non-polar environment and restrict the free rotation of the guest molecules, hence, the absorption and emission intensities of the SR7B molecule was changed [16-22]. The absorption and emission spectral shifts and shape of SR7B with α-CD or β-CD are the same indicating that both CDs form a similar type of inclusion complex. Binding constant (Table 1) for the inclusion complexes was determined from the slope and intercept of the plot $1/(A-A_0)$ vs 1/[CD] and $1/(I-I_0)$ vs 1/[CD]. The straight line of the plot and the presence of an isosbestic point in the absorption spectrum suggest the formation of a 1: 1 inclusion complex [16-22].

## 3.2. Molecular Modeling

The ground state geometries of SR7B, α-CD, β-CD and their inclusion complexes were optimized by the PM3 method. HOMO, LUMO (Figure 4), energy, enthalpy, entropy, free energy, dipole moment and zero-point vibrational energy values for SR7B, α-CD, β-CD and the inclusion complexes are all listed in Table 2. When SR7B entered the CD cavity, the polarity and the above parameter values for SR7B, α-CD, and β-CD significantly changed in the inclusion complexes. The internal diameter of the α-CD and β-CD is approximately 5.6 and 6.5 Å and the height is 7.8 Å respectively. In SR7B, the horizontal bond length is 15.58 Å and the vertical bond distance is 8.63 Å (Table 2 and Figure 4). In SR7B, horizontal bond length and the vertical bond length of the N-ethyl naphthalen-2-amine ring is longer than the α-CD and β-CD cavity size, hence, this molecule is partially encapsulated in the CD cavity [43-50].

The ΔE, ΔG and ΔH values for the SR7B/β-CD inclusion complex are more negative than SR7B/α-CD and the cavity.

The negative Gibbs energy and enthalpy of the inclusion complexes indicate that the formation of the complex is spontaneous and exothermic. The negative entropy (ΔS) value suggests the disorder of the system. The energy gap between HOMO and LUMO of the complexes suggest that there will be a significant change in the electronic structures of the guest molecules while molecular recognition and binding. The red color in the molecular electrostatic potential's (MEP) figure (Figure 4) shows that the electronegative charge of the atoms is greater than that of other atoms. HOMO-LUMO gap for SR7B/β-CD inclusion complex was more negative, which supports that this complex is more stable than SR7B/α-CD inclusion complexes.

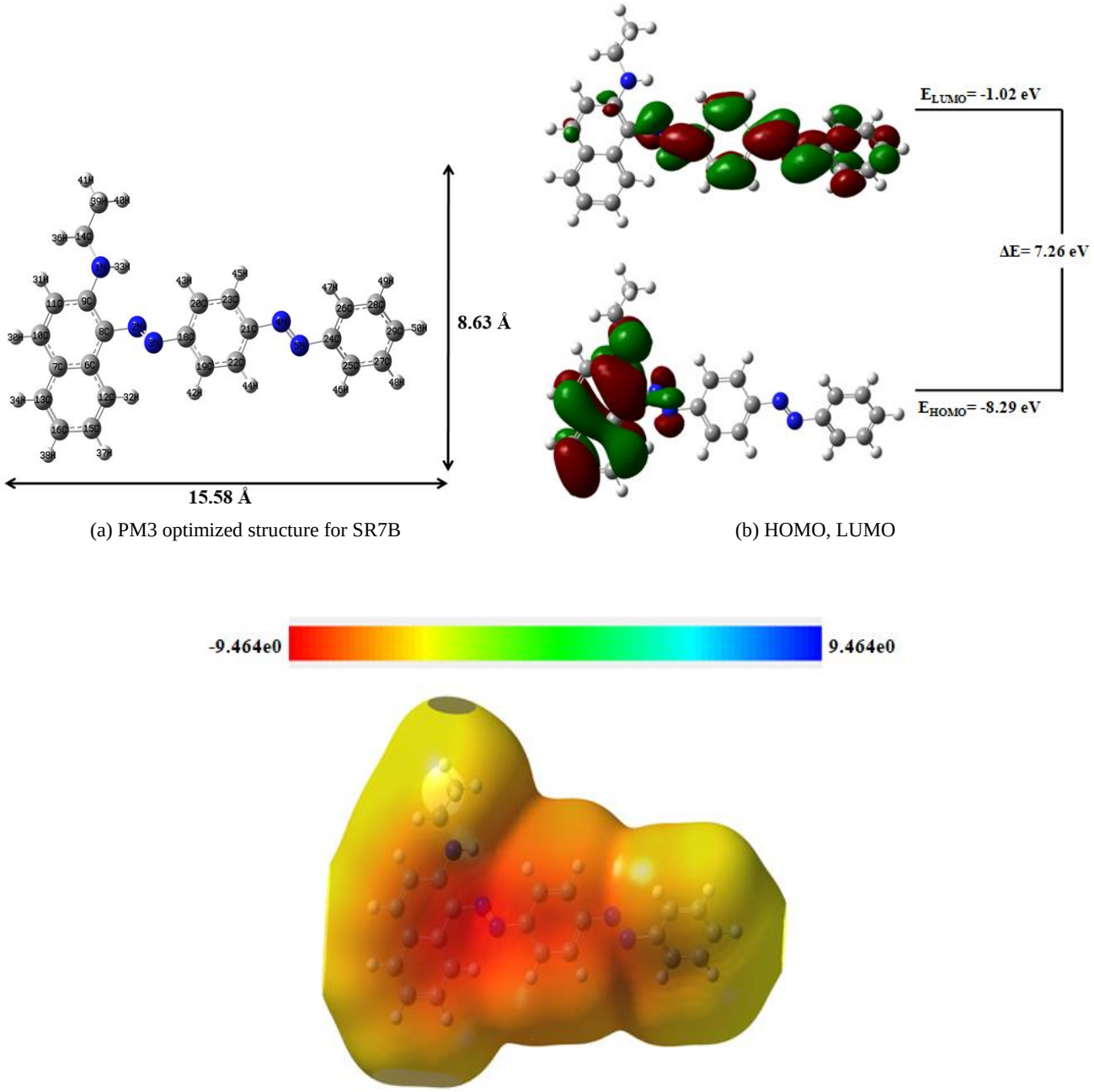


(a) PM3 optimized structure for SR7B

(b) HOMO, LUMO

(c) MEP

***Figure 4.*** *PM3 optimized structures of (a) SR7B, (b) HOMO, LUMO and (c) MEP of SR7B. The blue color indicates for nitrogen atom, while in HOMO-LUMO, the green and red colors denote negative and positive phases of the molecules.*

***Table 2.*** *Energetic features, thermodynamic parameters and HOMO-LUMO energy calculations for SR7B and its inclusion complexes by semiempirical PM3 method.*

| Properties | SR7B | α-CD | β-CD | SR7B/α-CD | SR7B/β-CD |
|---|---|---|---|---|---|
| $E_{HOMO}$ (eV) | -8.29 | -10.37 | -10.35 | -8.42 | -8.44 |
| $E_{LUMO}$ (eV) | -1.02 | 1.26 | 1.23 | -1.22 | -1.32 |
| $E_{HOMO} - E_{LUMO}$ (eV) | 7.26 | -11.63 | -11.58 | 7.19 | 7.12 |
| Dipole (D) | 1.46 | 11.34 | 12.29 | 10.96 | 10.56 |
| E (kcal $mol^{-1}$) | -170.91 | -1247.62 | -1457.63 | -1083.08 | -1295.89 |
| ΔE (kcal $mol^{-1}$) | - | - | - | -6.37 | -9.17 |
| G (kcal $mol^{-1}$) | -266.73 | -676.37 | -789.52 | -945.25 | -1002.41 |
| ΔG (kcal $mol^{-1}$) | - | - | - | -2.15 | -53.84 |
| H (kcal $mol^{-1}$) | -210.97 | -570.84 | -667.55 | -796.77 | -852.93 |
| ΔH (kcal $mol^{-1}$) | - | - | - | -14.96 | -25.59 |
| S (kcal/mol-Kelvin) | 0.187 | 0.353 | 0.409 | 0.498 | 0.561 |
| ΔS (kcal/mol-Kelvin) | - | - | - | 0.042 | 0.035 |
| ZPE | 250.16 | 635.09 | 740.56 | 886.52 | 941.11 |

kcal/mol; **kcal/mol-Kelvin; ZPE = Zero-point vibration energy

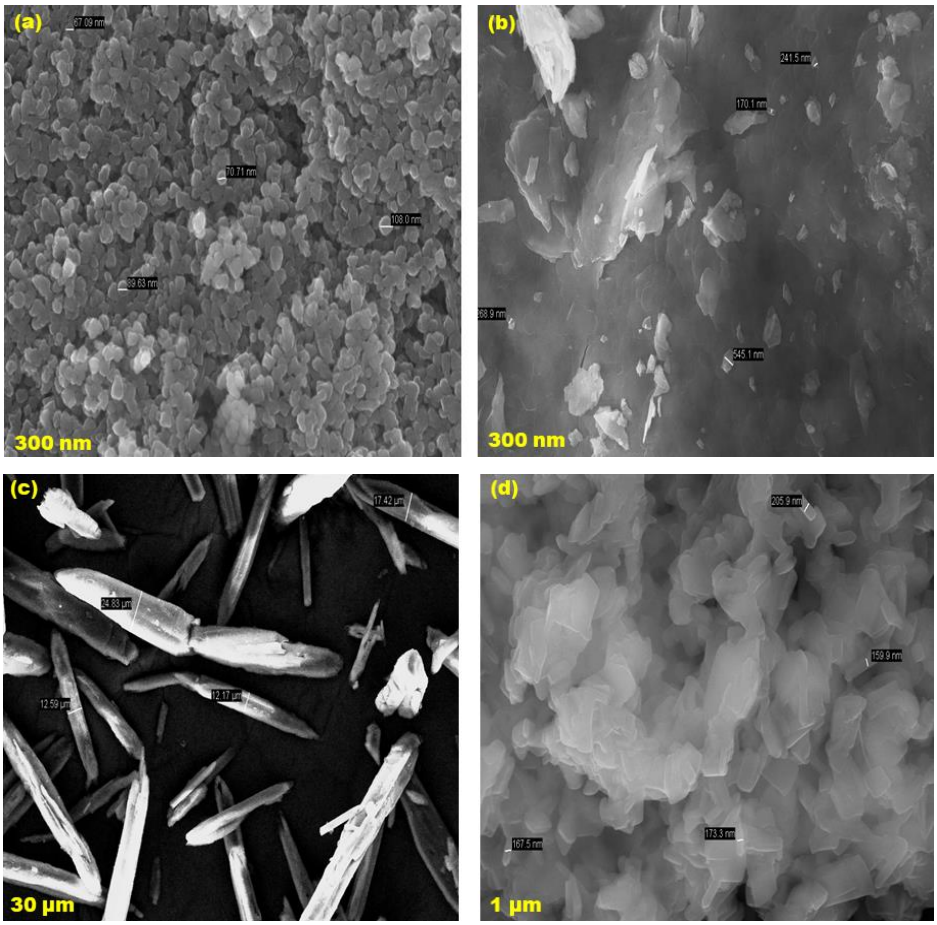


***Figure 5.*** *FE-SEM images for (a) ZnO, (b) ZnO/β-CD, (c) SR7B, (d) ZnO/SR7B/β-CD inclusion complexes.*

### 3.3. Doping Effect of SR7B/ CD on ZnO Nanoparticles

In the solution phase, the absorption and emission spectra of the ZnO, ZnO/SR7B, ZnO/β-CD, SR7B/CD/ZnO nanoparticles are determined. The ground and excited state bands of ZnO nanoparticles appear at 320 nm and 420, 355 nm, respectively [36-38]. When SR7B solution was added to the ZnO nanoparticle solution, the above ground and excited state bands red shifted to 588, 377 nm and 435 nm, respectively. With the addition of β-CD solution to the ZnO nano, the ground and excited state band shifted to 250 and 398 nm, respectively. When SR7B/β-CD solution was added to the ZnO nanoparticles, the ground and excited state bands shifted to 350, 240 nm and 405 nm, respectively. The above red or blue shifts in the ground and excited state spectra suggest that SR7B and CD are doped on ZnO nanoparticles. Generally, if other nano doped/covered the ZnO nanoparticles, the intensity tends to increase or decrease and the interaction is supported by spectral variations.

### 3.4. FE-SEM and TEM Images

ZnO nano, SR7B, ZnO/β-CD and SR7B/CD/ZnO nanomaterials were examined by FE-SEM and EDAX (Figure 5). ZnO particles form small size balls present in cluster shape, ZnO/β-CD is appear in sheet shape, SR7B is present in microrod shape and SR7B/CD/ZnO present in marble rod shape image. FE-SEM-EDAX data shows (a) ZnO nano contains 57.34% zinc nano and 42.66% oxygen, (b) ZnO/β-CD nano comprises 19.67% zinc, 54.42% oxygen and 25.91% carbon, (c) SR7B dye contains 79.17% carbon, 20.83% nitrogen, and (d) SR7B/CD/ZnO contains 2.72% zinc, 66.15% carbon, 13.70% nitrogen, and 17.44% oxygen. FE-SEM pictures and the atom composition of the nano ZnO, SR7B are different from SR7B/CD/ZnO, confirming the formation of new nanomaterials.

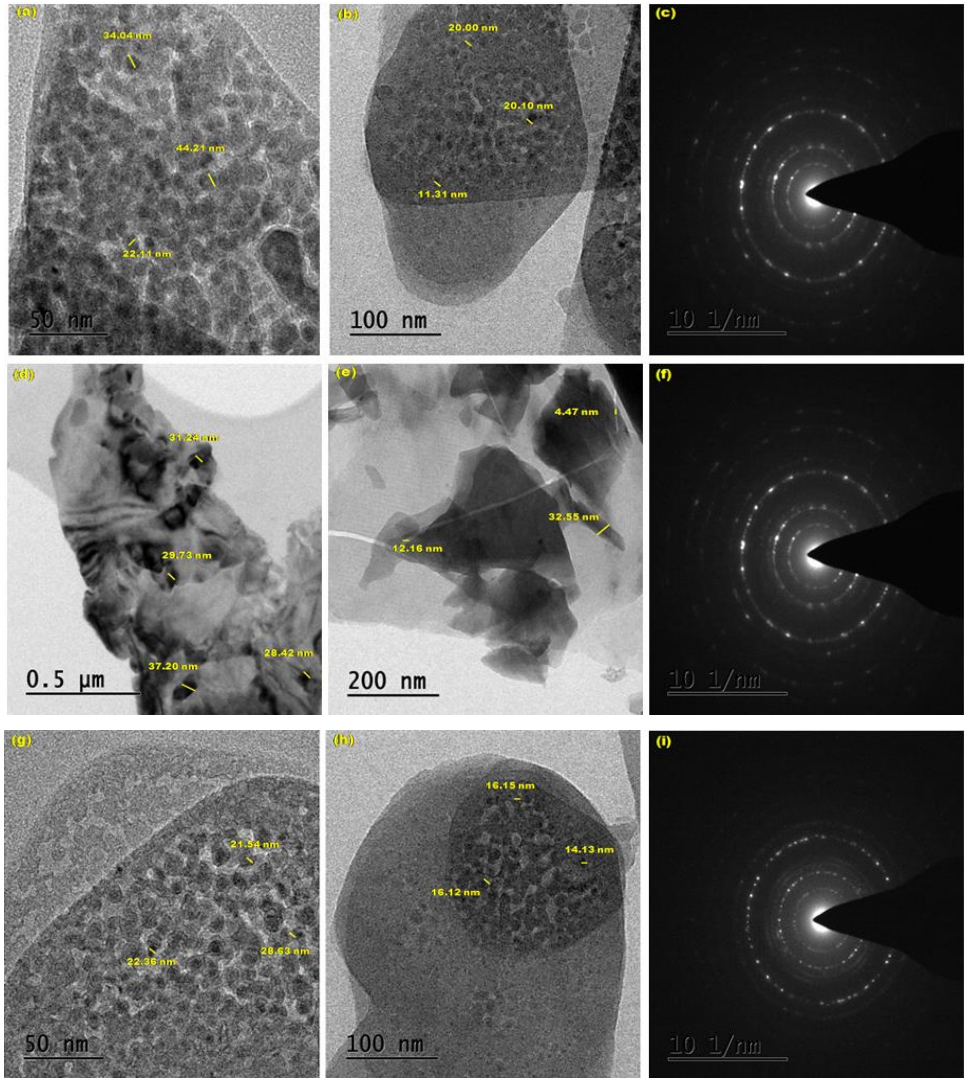


***Figure 6.*** *HR-TEM images for (a-c) ZnO, (d-f) ZnO/β-CD, (g-i) ZnO/SR7B/β-CD.*

TEM images of ZnO, ZnO/β-CD and SR7B/CD/ZnO are displayed in Figure. 6. Nanosheet like structures found in the ZnO nanomaterials, while nanorod like structure is formed in ZnO/β-CD. TEM image of ZnO nanosheet showed uniformly spherical particles between 20 and 44 nm in size and ZnO/β-CD nano, the particles size between 20 and 40 nm. The SR7B/CD/ZnO nano-sheet image was displayed between 14-16 nm. The formation of nanoparticles is supported by TEM-EDX data: (a) ZnO nano contains 69.84% zinc nano and 30.16% oxygen, (b) ZnO/β-CD nano comprises 8.79% zinc, 44.59% oxygen and 46.61% carbon, (c)) The composition of SR7B/CD/ZnO is 25.11% zinc, 24.46% carbon, 46.86% oxygen, and 3.57% nitrogen. The presence of ZnO along with SR7B/β-CD is confirmed by the EDX data for the metallic nanoparticles.

The nanoparticle size is analyzed by X-RD and HR TEM methods. In XRD method, Scherer equation is used and the particle size is given below: ZnO nano – 19.30 nm, β-CD – 23.84, SR7B- 20.29 nm, ZnO/β-CD - 20.69 nm, and SR7B/CD/ZnO Nano – 14.92 nm. In HR-TEM, the particle size is measured by using IMAGE-J software and the average particle size is calculated by origin software. ZnO nano– 24.98 nm, ZnO/β-CD– 23.98 nm, SR7B/CD/ZnO nano– 19.31 nm. Compared to XRD method, the 5-7 nm particle size is varied in HR-TEM method.

## 3.5. Powder X-RD

XRD method provided additional confirmation of the formation of nanomaterials. With the use of the JCPDS: 03-065-3411 data, the mineral name (3C) and the development of the hexagonal closely packed (HCP) structure have been confirmed. The JCPDS card number 800-075 was used to index and all the diffraction peaks conformed with its standard ZnO face-centered cubic peaks. The values of the hkl plane are found at (100), (002), (101), (102), (103), (110), (112) and (201) reflection planes of the hexagonal structure of ZnO.

In ZnO, eight diffraction peaks located at 31.80, 34.51, 36.21, 47.52, 56.61, 62.90, 67.91, 69.92 correspond to the reflection planes of hexagonal structure of ZnO. In β-CD, eight peaks were observed at 13.39, 19.93, 23.50, 27.65, 31.96, 35.54, 40.58, 48.90, while in ZnO/β-CD ten peaks formed at 10.15, 15.18, 25.41, 28.38, 34.92, 42.29, 49.77, 59.16, 63.32, 70.33. In SR7B, seven peaks formed at 14.21, 15.55, 19.20, 24.46, 25.94, 27.69, whereas in SR7B/CD/ZnO eleven peaks were noted at 8.30, 16.80, 21.64, 26.62, 28.51, 33.10, 35.15, 42.40, 49.94, 58.90, 63.50. Compared to isolated SR7B, the XRD patterns of the SR7B/CD/ZnO nanomaterials showed a different diffraction pattern and different peak intensities, suggesting that inclusion complex nanomaterials were formed. Further, several prominent peaks appeared from 10 to 80 degree range, supporting the formation of SR7B/CD/ZnO inclusion complex nanomaterials.

## 3.6 Infrared Spectral Studies

FTIR spectra of ZnO nano, SR7B, ZnO/SR7B, ZnO/β-CD and SR7B/CD/ZnO were analysed. Due to the conversion of $Zn^{+2}$ to ZnO nanoparticles, the FTIR frequencies of the ZnO nanoparticles were observed at 3325, 1587, 1450, 592, and 513 $cm^{-1}$. The frequencies appear at 3325 $cm^{-1}$ indicate the presence of ZnO and the peaks seen at 592, and 513 $cm^{-1}$ suggest the presence of Zn nanoparticles. It is already reported, the FTIR spectrum of pure ZnO nanoparticles peaks at 595 $cm^{-1}$, which is characteristic of ZnO band and the broad band peak noted at 3507 $cm^{-1}$ can be attributed to the characteristic absorption of O-H group. When zinc oxide nano added to β-CD, the 3325 $cm^{-1}$ frequency shifted to 3280 $cm^{-1}$, while 1587, 1450 $cm^{-1}$ frequencies moved to 1614, 1514 $cm^{-1}$ and 592, 513 $cm^{-1}$ peaks shifted to 594, 526 $cm^{-1}$. The above variation in the FTIR frequencies indicates that the CD is covered on ZnO nanoparticles.

In SR7B, NH group stretching frequency appears at 3051 $cm^{-1}$, azo group stretching frequency seen at 1365 $cm^{-1}$, aromatic ring stretching frequency appears at 2970, 1433 $cm^{-1}$. C-NH frequency appears at 1122 $cm^{-1}$, and CH out of plane bending frequency looks at 738, 684 $cm^{-1}$. Out of plane bending frequency seems at 850, 808 $cm^{-1}$ and C-N-C bending frequency appear at 532 $cm^{-1}$. When SR7B/β-CD doped on ZnO nano particles, the above frequencies are shifted to lower or higher wave numbers. In ZnO/SR7B/CD, NH group stretching frequency appears at 3292 $cm^{-1}$, azo group stretching frequency appears at 1367 $cm^{-1}$, aromatic ring stretching frequency seems at 2973, 1435 $cm^{-1}$. C-NH frequency looks at 1118 $cm^{-1}$, and CH out of plane bending frequency appears at 738, 682 $cm^{-1}$. Out of plane bending frequency seems at 958, 846 $cm^{-1}$ and C-N-C bending frequency looks at 597 $cm^{-1}$. Compared to SR7B and ZnO/β-CD, the SR7B/CD/ZnO nanomaterials showed a marked change in the frequencies, suggesting that the SR7B/β-CD was doped on ZnO nanoparticles.

## 3.7. DTA Thermogram

DTA profiles of pure ZnO nano, SR7B, ZnO/β-CD and SR7B/CD/ZnO are analyzed. In ZnO nano, two exothermic and three endothermic peaks were noticed at 226.1, 546.7 ℃ and 272.6, 731.1, 19.2 ℃, respectively. SR7B exhibits one exothermic and one endothermic peak at 240.6 ℃ and 597.8°C, respectively. β-CD exhibits four exothermic peaks at 230.3, 515.6, 657.4, 761.8°C. In ZnO/β-CD, two exothermic and four endothermic peaks appear at 224.3, 932.4 ℃ and 265.2, 354.6, 749.8, 884.1 ℃, respectively. In SR7B/CD/ZnO, two endothermic and three exothermic peaks appear at 280.5, 898.8 ℃, and 236.7, 745.3, 966.8 ℃, respectively. The endothermic peaks in the nanomaterials are caused by the loss of water from the CDs. In contrast to the pure SR7B and ZnO, a

new peak arises in SR7B/CD/ZnO, indicating the formation of the new nanomaterials.

## 4. Conclusion

Sudan Red-7B/Cyclodextrin doped ZnO nanocomposites are synthesized and analysed by various spectral and microscopic methods. The solvent and CD studies show that the azo-imino tautomer is present in SR7B molecule and depend upon the polarity of the solvents, the absorbance and emission intensities of the azo-imino tautomer are varied. Horizontal bond length of SR7B is longer than the CD cavities, hence, this molecule is partially encapsulated in the CD cavity. HOMO-LUMO gap for SR7B/β-CD inclusion complex is more negative than SR7B/α-CD, suggesting the previous inclusion complex is more stable than the latter. Red or blue shifted absorption and fluorescence maxima were seen in SR7B/CD/ZnO nanocomposites than SR7B/CD. TEM image showed that nanosheets are formed in SR7B/CD/ZnO. Compared to the XRD method, the 5-7 nm particle size of SR7B/CD/ZnO is varied in HR-TEM method.

## Abbreviations

| | |
|---|---|
| FTIR | Fourier Transform Infrared Spectroscopy |
| DTA | Differential Thermal Analysis |
| XRD | X-ray Diffraction |
| SEM | Scanning Electron Microscopy |
| TEM | Transmission Electron Microscopy |
| HOMO | Highest Occupied Molecular Orbital |
| LUMO | Lowest Unoccupied Molecular Orbital |
| SR7B | Sudan Red 7B |
| ZnO NPs | Zinc Oxide Nanoparticles |
| α-CD | Alpha Cyclodextrin |
| β-CD | Beta Cyclodextrin |
| PM3 | Parametric Method 3 |
| ΔE | Internal Energy Change |
| ΔH | Enthalpy Change |
| ΔG | Free Energy Change |
| ΔS | Entropy Change |

## Author Contributions

The authors confirm contributions to the paper as follows: P. Ramasamy - Experimental study: A. Mani, - Calculation, Analysis, Data Collection, A. Antony Muthu Prabhu, G. Venkatesh – PM3 calculation, Data interpretation, Manuscript draft preparation, Supervisor-N. Rajendiran.

## Acknowledgments

This work was supported by the Rashtriya Uchchatar Shiksha Abhiyan (RUSA) Phase -2.0 [No. 128/A1/ RUSA 2.0, Health and Environment] New Delhi, India.

## Data Availability

No data was used for the research described in the article.

## Conflicts of Interest

The authors declare no conflicts of interest.

## References

[1] Zince, T., Bindenwald, M. On the Action of Phosphoryl Bromide on Aromatic Amines. *Chem Ber* 1884, 17, 3026-33. https://doi.org/10.1002/cber.188401702282

[2] Richard Kuhn, Friedrich Bär, On Chinophthalone, *Annalen* 1935, 516, 143-161, https://doi.org/10.1002/jlac.19355160109

[3] Frierz-David, H. E., Blangey, L., Streif, H. On the Knowledge of p-Hydroxy Azo Dye, *Helvetica Chimica Acta* 1946, 29, 1718-64. https://doi.org/10.3929/ethz-a-000091735

[4] Kishimoto, S., Kitahara S., Manabe O., Hiyama H. Tautomerism and Dissociation of 4-Arylazo-1-Naphthols in Various Solvents, *J. Org Chem* 1978, 43, 3882-86; https://doi.org/10.1021/jo00414a018

[5] Antonov, L., Stoyanov, S., Stoyanov, T. Quantitative analysis of tautomeric equilibrium in 1-phenylazo-4-naphthols—a new approach, *Dyes and Pigments*, 1994, 26, 149-158. https://doi.org/10.1016/0143-7208(94)85008-9

[6] Antonov, L., Stoyanov, S. 1-Naphthol. Dyes and Pigments, *Dyes and Pigments*, 1995, 28, 31-39. https://doi.org/10.1016/0143-7208(94)00076-E

[7] Antonov, L., Fabian, W. M. F., Nedeltcheva, D., Kamounah, F. S. Tautomerism of 2-hydroxy naphthaldehyde Schiff bases. *J. Chem. Soc., Perkin Trans.* 2, 2000, 1173–1179. https://doi.org/10.1039/B000798F

[8] Antonov, L., Stoyanov, S., Stoyanova, T. Tautomeric equilibrium in 1-phenylazo-2-naphthol—A quantitative study, *Dyes and Pigments* 1995, 27, 133-142. https://doi.org/10.1016/0143-7208(94)00042-Z

[9] Antonova, L., Kawauchib, S., Satohb, M., Komiyama, J. Ab initio modeling of the solvent influence on the azo-hydrazone tautomerism, *Dyes and Pigments* 1999, 40, 163-170.

[10] Joshi, H., Kamounah, F. S., van der Zwan, G., Gooijer, C., Antonov, L. Temperature dependent absorption spectroscopy of some tautomeric azo dyes and Schiff bases. *J Chem Soc Perkin Trans 2:* 2001, 2303-08. https://doi.org/10.1007/s11661-015-3061-7

[11] Hem Joshi, Fadhil S. Kamounah, Cees Gooijera, Gert van der Zwan, Liudmi Antonov, Excited state intramolecular proton transfer in some tautomeric azo dyes and Schiff bases containing an intramolecular hydrogen bond. *J. Photochem. and Photobiol. A: Chem.* 2002, 152, 183–191.

[12] Fadhil S. Kamounah, Liudmi Antonov, Vesselin Petrov, Gert van der Zwan, An integrated approach to the study of the tautomerism of 4-((Phenylimino) methyl) naphthalene-1-ol, *J. Phys. Org. Chem.* 2007, 20, 313–320. https://doi.org/10.1002/poc.1143

[13] Zollinger, H. Color Chemistry: Syntheses, Properties and Applications of Organic Dyes and Pigments. VCH, Weinheim 1991.

[14] Smoluch, M., Joshi, H., Gerssen, A., Gooijer, C. van der Zwan, G., Fast excited-state intramolecular proton transfer and sub nanosecond dynamic Stokes shift of time-resolved fluorescence spectra of the 5-methoxysalicylic acid/diethyl ether complex. *J. Phys. Chem.* 2005, 109, 535–541. https://doi.org/10.1021/jp0475281

[15] Alarcón, S. H., Olivieri, A. C., Labadie, G. R., Cravero, R. M., Gonzales-Sierra, M. Tautomerism of representative aromatic—hydroxy carbaldehyde anils as studied by spectroscopic methods and AM1 calculations. Synthesis of 10-hydroxyphenanthrene-9-carbaldehyde. *Tetrahedron.* 1995, 51, 4619–4626. https://doi.org/10.1016/0040-4020(95)00002-P

[16] Antony Muthu Prabhu, A., Venkatesh, G., Sankaranarayanan, R. K., Rajendiran, N. Azonium-ammonium tautomerism and inclusion complexation of 4-amino-2',3-dimethyl azobenzene. *Indian J. Chem.* 2010, 49A, 407–417. http://nopr.niscpr.res.in/handle/123456789/7824

[17] Venkatesh, G., Sankaranarayanan, R. K., Antony Muthu Prabhu, A., Rajendiran, N. Azonium-Ammonium Tautomerism and Inclusion Complexation of 1-(2, 4-diamino phenylazo) naphthalene and 4-amino azobenzene. *J. Fluores.* 2011, 21, 1485-1497. https://doi.org/10.1007/s10895-011-0835-1

[18] Prema Kumari, J., Antony Muthu Prabhu, A., Venkatesh, G., Subramanian, V. K., Rajendiran, N. Effect of solvents and pH on β-CD Inclusion complexation of 2, 4-dihydroxy azobenzene and 4-hydroxy azobenzene. *J. Solution Chem,* 2011, 40, 327–347. https://doi.org/10.1007/s10953-010-9639-1

[19] Venkatesh, G., Saravanan, J., Rajendiran, N. Cyclodextrin covered organic micro rod and micro sheet derived from supramolecular self-assembly of 2, 4-dihydroxy azobenzene and 4-hydroxy azobenzene inclusion complexes. *Bull. Chem. Soc. Jpn.* 2014, 87, 283-293. https://doi.org/10.1246/bcsj.20130255

[20] Rajendiran, N., Venkatesh, G., Saravanan, J. Encapsulation of thiazoresorcinol and thiazocresol dye within α- and β-CD cavities: Spectral and molecular modeling studies. *J. Mol. Struc.* 2014, 1072, 242-252. https://doi.org/10.1016/j.molstruc.2014.05.018

[21] Antony Muthu Prabhu, A., Venkatesh, G. Rajendiran, N. Azo-Hydrazo tautomerism in 1-phenyazo-2-naphthol dyes in various solvents, pH and β-CD. *J. Fluorescence,* 2010, 20, 961–972. https://doi.org/10.1007/s10895-010-0642-0

[22] Rajendiran, N., Sankaranarayanan, R. K. Azo dye/Cyclodextrin: New findings of identical nanorods through 2: 2 inclusion complexes. *Carbohydrate Polymers,* 2014, 106, 422-431. https://doi.org/10.1016/j.carbpol.2014.01.030

[23] Supraja, N., Prasad, T. N. V. K. V., Giridhara Krishna, T. David, E. Synthesis, characterization, and evaluation of the antimicrobial efficacy of Boswellia ovalifoliolata stem bark-extract-mediated zinc oxide nanoparticles. *Appl. Nanosci.* 2016, 6, 581–590, https://doi.org/10.1007/s13204-015-0472-0

[24] Niranjan Bala, S. Saha, M. Chakraborty, M. Maiti, S. Das, R. Basub, P. Nandy, Green synthesis of zinc oxide nanoparticles using Hibiscus subdariffa leaf extract: effect of temperature on synthesis, anti-bacterial activity and anti-diabetic activity. *RSC Adv.*, 2015, 5, 4993–5003. https://doi.org/10.1039/c4ra12784f

[25] Xiong, H. M. ZnO Nanoparticles Applied to Bioimaging and Drug Delivery, *Adv. Mater.*, 2013, 25(37), 5329–5335. https://doi.org/10.1002/adma.201301732

[26] Sharmaa, D., Rajputa, J., Kaitha, B. S., Kaurb, M. Synthesis of ZnO nanoparticles and study of their antibacterial and antifungal properties. *Thin Solid Films,* 2010, 519(3), 1224-1229. https://doi.org/10.1016/j.tsf.2010.08.073

[27] Nair, S. Role of size scale of ZnO nanoparticles and microparticles on toxicity toward bacteria and osteoblast cancer cells. *J. Mater. Sci.: Mater. Med.*, 2009, 20 (Suppl. 1), S 235–S241. https://doi.org/10.1007/s10856-008-3548-5

[28] Kirthi, A. V., Rahuman, A. A., Rajakumar, G., Marimuthu, S. Acaricidal, pediculocidal and larvicidal activity of synthesized ZnO nanoparticles using wet chemical route against blood feeding parasites. *Parasitol. Res.*, 2011, 109, 461–472. https://doi.org/10.1007/s00436-011-2277-8

[29] Alkaladi, A., Abdelazim, A. M., Afifi, M. Antidiabetic Activity of Zinc Oxide and Silver Nanoparticles on Streptozotocin-Induced Diabetic Rats. *Int. J. Mol. Sci.*, 2014, 15, 2015–2023. https://doi.org/10.3390/ijms15022015

[30] Dagdeviren, C., Hwang, S. W., Su, Y., Kim, S. Transient, Biocompatible Electronics and Energy Harvesters Based on ZnO. *Small,* 2013, 9(20), 3398–3404. https://doi.org/10.1002/smll.201300146

[31] Zhang, Yuanyuan, Leu, Yu-Rui, Aitken J. Robert Riediker Michael, Inventory of Engineered Nanoparticle-Containing Consumer Products Available in the Singapore Retail Market and Likelihood of Release into the Aquatic Environment. *International J Environmental Research and Public Health.* 2015, 12, 8717–8743. https://doi.org/10.3390/ijerph120808717

[32] Wang, L., Kang, Y., Liu, X., Zhang, S. ZnO nanorod gas sensor for ethanol detection. *Sens. Actuators, B,* 2012, 162(1), 237–243. https://doi.org/10.1016/j.snb.2011.12.073

[33] Cross, S. E., Innes, B., Roberts, M. S., Tsuzuki, T. Human skin penetration of sunscreen nanoparticles: in vitro assessment of a novel micronized zinc oxide formulation, Skin Pharmacol. *Physiol.*, 2007, 20(3), 148–154. https://doi.org/10.1159/000098701

[34] Zhou, J., Xu, N., Wang, Z. L. Dissolving behavior and stability of ZnO wires in biofluids: a study on biodegradability and biocompatibility of ZnO nanostructures. *Adv. Mater.*, 2006, 18(18), 2432–2435. https://doi.org/10.1002/adma.200600200

[35] Rasmussen, J. W., Martinez, E., Louka, P., Wingett, D. G. Zinc oxide nanoparticles for selective destruction of tumor cells and potential for drug delivery applications. *Expert Opin. Drug Delivery*, 2010, 7(9), 1063–1077. https://doi.org/10.1517/17425247.2010.502560

[36] Siva Kumar, Surabhi, Putcha Venkateswarlu, Vanka Ranga Rao, Gollapalli Nageswara Rao, Synthesis, characterization and optical properties of zinc oxide nanoparticles. *International Nano Letters*, 2013, 3, 30-35. https://doi.org/10.1186/2228-5326-3-30

[37] Sukesh Kashiram Tumram, Rajdip Bandyopadhyaya, Zinc oxide nanostructures: Experiments probing their transformation to nanorods. *Materials Science and Engineering: B*, 2023, 296, 116569- 74. https://doi.org/10.1016/j.mseb.2023.116569

[38] Ramasamy, P., Mani, A., Sneha, B., Nivetha, E., Venkatesan, M., Rajendiran, N. Azo-hydrazo tautomerism in Sudan Red-B and Cyclodextrin/Sudan Red-B doped ZnO nanomaterials. *J Molecular Structure, 2025;* 1329: 141423-32. https://doi.org/10.1016/j.molstruc.2025.141423

[39] Mani, A., Ramasamy, P., Antony Muthu Prabhu, A., Rajendiran, N. Investigation of Ag and Ag/Co bimetallic nanoparticles with naproxen-cyclodextrin inclusion complex. *J. Molecular Structure 2023;* 1284: 135301-10. https://doi.org/10.1016/j.molstruc.2023.135301

[40] Mani, A., Venkatesh, G., Senthilraja, P., Rajendiran, N. Synthesis and Characterisation of Ag-Co-Venlafaxine-Cyclodextrin Nanorods. *European J Advanced Chemistry Research, 2024;* 5: 9-16. https://doi.org/10.24018/ejchem.2024.5.1.147

[41] Mani, A., Ramasamy, P., Antony Muthu Prabhu, A., Senthilraja, P., Rajendiran, N. Synthesis and Analysis of Ag/Olanzapine /Cyclodextrin and Ag/Co/Olanzapine /Cyclodextrin Inclusion Complex Nanorods. *Physics and Chemistry of Liquids, 2024;* 62: 196-209. https://doi.org/10.1080/00319104.2023.2297223

[42] Mani, A., Ramasamy, P., Antony Muthu Prabhu, A., Senthilraja, P., Rajendiran, N. Synthesis and Characterisation of Ag/Co/Chloroquine/Cyclodextrin Inclusion Complex Nanomaterials. *J Sol-Gel Science and Technology*, 2025. https://doi.org/10.1007/s10971-024-06620-5

[43] Prema Kumari, J., Antony Muthu Prabhu, A., Venkatesh, G., Subramanian, V. K., Rajendiran, N. Spectral characteristics of sulfadiazine, sulfisomidine: Effect of solvents, pH and β-CD. *Physics and Chemistry of Liquids*, 2011, 49, 108–132. https://doi.org/10.1080/00319104.2010.509724

[44] Jude Jenita, M., Antony Muthu Prabhu, A., Rajendiran, N. Theoretical study of inclusion complexation of tricyclic antidepressant drugs with β-CD. *Indian J. Chemistry A*, 2012, 51 A, 1686-1694.

[45] Rajendiran, N., Saravanan, J. Inclusion complexation of sulfa pyridine with α- and β-CDs: Spectral and molecular modeling study. *J. Molecular Structure*, 2013, 1054-1055 215–222. https://doi.org/10.1016/j.molstruc.2013.09.035

[46] Antony Muthu Prabhu, A., Rajendiran, N., Encapsulation of labetalol, and pseudoephedrine in β-CD cavity: Spectral and molecular modeling studies. *J. Fluorescence*, 2012, 22, 1461-1474. https://doi.org/10.1007/s10895-012-1083-8

[47] Rajendiran, N., Sankaranarayanan, R. K., Saravanan, J. A study of supramolecular host–guest interaction of dothiepin and doxepin drugs with cyclodextrin macrocycles. *J Molecular Structure*, 2014, 106, 7252-260. https://doi.org/10.1016/j.molstruc.2014.03.051

[48] Rajendiran, N., Venkatesh, G., Saravanan, J. Supramolecular aggregates formed by sulfadiazine and sulfisomidine inclusion complexes with α- and β-cyclodextrin. *Spectrochimica Acta, A*, 2014, 129, 157-162, https://doi.org/10.1016/j.saa.2014.03.028

[49] Rajendiran, N., Venkatesh, G., Mohandoss, T. Fabrication of 2 D nano sheet through self assembly behavior of sulfamethoxy pyridazine inclusion complex with α- and β-cyclodextrins. *Spectrochim Acta A*, 2014, 123, 158-166, https://doi.org/10.1016/j.saa.2013.12.053

[50] Rajendiran, N., Sankaranarayanan, R. K., Venkatesh, G. Excimer emission in inclusion complexes of dibenzofuran and 5-dibenzosuberenone with α- and β-cyclodextrins. Bull Chem Soc Japan, 2014, 87, 797-808. https://doi.org/10.1246/bcsj.20140057